Formation Mechanism and Porosity Development in Porous Boron Nitride

Anouk L'Hermitte [1,2], Daniel M. Dawson [3], Pilar Ferrer [4], Kanak Roy [4,†], Georg Held [4], Tian Tian [1], Sharon E. Ashbrook [3] and Camille Petit [1*]*

[1] Barrer Centre, Department of Chemical Engineering, Imperial College London, London SW7 2AZ, United Kingdom

[2] Department of Materials, Imperial College London, London SW7 2AZ, United Kingdom

[3] School of Chemistry, EaStCHEM and Centre of Magnetic Resonance, University of St. Andrews, North Haugh, St. Andrews, Fife KY16 9ST, United Kingdom

[4] Diamond Light Source Ltd., Diamond House, Harwell Science and Innovation Campus, Didcot OX11 0DE, United Kingdom

[†] Current address: Department of Chemistry, Banaras Hindu University, Varanasi, Uttar Pradesh 221005, India

* Corresponding authors: Camille Petit (email: camille.petit@imperial.ac.uk, +44 (0)20 7594 3182); Sharon E. Ashbrook (email: sema@st-andrews.ac.uk, +44 (0)13 3446 3779)

KEYWORDS: boron nitride, porosity, formation mechanism, adsorption, materials characterisation, spectroscopy

ABSTRACT

Porous boron nitride (BN) has proven promising as a novel class of inorganic materials in the field of separations and particularly adsorption. Owing to its high surface area and thermal stability, porous BN has been researched for CO_2 capture and water cleaning, for instance. However, research remains at laboratory scale due to a lack of understanding of the formation mechanism of porous BN, which is largely a 'black box' and prevents scale-up. Partial reaction pathways have been unveiled, but they omit critical steps in the formation, including the porosity development, which is key to adsorption. To unlock the potential of porous BN at a larger scale, we have investigated its formation from the perspective of both chemical formation and porosity development. We have characterised reaction intermediates obtained at different temperatures with a range of analytical and spectroscopic tools. Using these analyses, we propose a mechanism highlighting the key stages of BN formation, including intermediates and gaseous species formed in the process. We identified the crucial formation of non-porous carbon nitride to form porous BN with release of porogens, such as CO_2. This work paves the way for the use of porous BN at industrial level for gas and liquid separations.

1. Introduction

Porous boron nitride (BN) has attracted wide attention in the past decade due to its promising properties for molecular separations[1-8] and more recently for photocatalysis.[9, 10] In the field of separation, porous BN benefits from high surface area up to 1900 $m^2 g^{-1}$, tuneable porosity,[11] and greater oxidative and thermal stability than common carbonaceous adsorbents.[12] Examples of gas sorption applications tested using porous BN include CO_2 capture,[1, 5] CO_2/CH_4 separation,[8] paraffin/olefin separation[7] and H_2 storage.[3, 6] Liquid separations tested using porous BN include water cleaning through removal of inorganic pollutants[3] and organic pollutants, such as solvents, dyes and oils.[2, 13]

The above-mentioned studies provide preliminary insights into the potential of porous BN. To ensure the deployment of the material at larger scale, one must be able to tune its properties for a given application, which clearly necessitates an understanding of its formation process. Few studies investigated the mechanism of porous BN formation via bottom-up synthesis.[1, 14-17] Most report the formation of hexagonal boron nitride (*h*-BN), a non-carbonaceous analogue of graphene with relatively low surface area (typically < 200 $m^2 g^{-1}$) and porosity compared to porous BN.[18, 19] In all the studies of porous BN, a few reactions have been suggested that account for the formation from boron- and nitrogen-containing precursors, but there is no consensus to date for a comprehensive reaction scheme with respect to the thermal treatment. In addition, reported syntheses use different reagents, gas atmospheres and reaction conditions, which impact the formation process and resulting product. Finally, different levels of purity are required, depending on the industrial application. Therefore, understanding how inherent oxygen and carbon impurities can be eliminated from the BN structure is critical.

Although no detailed formation mechanism has been confirmed and the synthesis parameter space (i.e., precursors, atmosphere, temperature) varies from study to study, two possible mechanisms to form porous or non-porous BN seem to emerge and were reported in a previous

study by O'Connor[20]: (i) nitridation of boron oxide with ammonia either from the reaction atmosphere or from decomposition of N-containing precursors and (ii) annealing of carbon nitride with boron from boron oxide. The two mechanisms may not be mutually exclusive and may also depend on the synthesis parameter space. Under the former mechanism fall, for instance, the studies by Brožek and Hubáček,[14] Ramirez Leyva et al.,[15] Wu et al.,[16] Tian et al. [17] and Hoffendahl et al.[21] The second category includes the work by Gong et al.,[22] who used graphene as a precursor. Hoffendahl et al.[21] indicated the formation of carbon nitride from melamine but referred to the reaction of boron oxide with ammonia to eventually form BN. Among all the above studies, only those of Ramirez Leyva et al.[15] and Tian et al.[17] cover the formation of porous BN and they link the porosity to gases released during the reaction, as also suggested by our earlier study.[1] A recent study by Höppe and Gross reports ammonium bis(biureto)borate as an intermediate in boron nitride formation using boric acid and urea under N_2.[23] In short, the formation mechanism of porous BN remains largely a 'black box'. Herein, we aim to address this knowledge gap by answering the following questions: What is the minimal temperature required to form porous BN? Which chemical intermediates are formed before obtaining porous BN? What is the influence of the precursors on the chemical and structural features of porous BN? We will also consider whether the two mechanisms mentioned earlier could take place concurrently in the reaction medium. To answer these questions, we focus on the formation mechanism based on the reaction of boric acid, melamine and urea heated up to 1050 °C under N_2 atmosphere, which consistently yields porous BN with high surface area, high pore volume and promising sorption performance.[11] To this end, we synthesised reaction intermediates at different temperatures up to 1050 °C. We investigated these intermediates with a variety of analytical and spectroscopic tools to propose a comprehensive formation mechanism of porous BN, paving the way for scale-up towards industrial applications.

2. Experimental Section

2.1. Synthesis of porous boron nitride and its reaction intermediates

The reagents boric acid (Sigma Aldrich, ACS reagent), melamine (Sigma Aldrich, 99%) and urea (Sigma Aldrich, molecular biology grade) were used with molar ratios of 1:1:5 following the multiple N-containing precursor synthesis previously developed in our group.[11] The three precursors were physically ground and mixed homogeneously for 3 min before being placed in an alumina crucible with the lid partially open to allow for any gas flow. The crucible was placed inside a horizontal tubular furnace in N_2 flow (BOC, zero grade, 99.998%). Each synthesis started with a 2 h purge at room temperature under N_2 with a flow rate of 250 cm^3 min^{-1}. After this step, the flow rate was lowered to 50 cm^3 min^{-1} and the temperature ramped up to 1050 °C at a rate of 10 °C min^{-1}. The complete synthesis of the porous BN material was obtained after a dwell time of 3.5 h at 1050 °C before cooling down, still under flowing N_2.

To investigate the nature of the reaction intermediates in the formation of porous BN, we carried out multiple syntheses based on the same initial mixture by programming the final temperature at: 100, 200, 300, 400, 600, 700, 800 and 900 °C. In the case of the intermediates, the furnace was allowed to cool down naturally as soon as the final temperature was reached to analyse the compounds present at this exact temperature during porous BN synthesis - neglecting any effect of the cooling down step. As a reference, the initial mixture was also analysed and referred to as the room temperature (RT) intermediate. Intermediate samples are referred to as "INT-X" where X corresponds to RT or the final temperature reached for each intermediate between 100 and 900 °C. Finally, we evaluated the impact of the 3.5-h dwell time at 1050 °C and synthesised an intermediate at 1050 °C with no dwell time before cooling. This sample is referred to as "BN-1050-t_0" as opposed to "BN-1050-$t_{3.5}$", which corresponds to our final product, porous BN. Note that when 1050 °C is mentioned in results without time

indication, this corresponds to the sample "BN-1050-$t_{3.5}$". After synthesis, all samples were stored in a desiccator at room temperature to enhance shelf-life and prevent any degradation from moisture.[24]

To compare the composition of relevant intermediates, carbon nitride (C_3N_4) was synthesised from melamine powder. Melamine was placed in an alumina crucible with the lid on, which was then placed inside a muffle furnace heated up to 560 °C with a heating rate of 5 °C min^{-1}. The final temperature was maintained for 4 h before the furnace was allowed to cool down naturally.

2.2 Characterisation

2.2.1 Chemical features of porous BN and its reaction intermediates

The samples were analysed using Fourier transform infrared (FTIR) spectroscopy. Each sample was ground in an agate mortar and spectra were collected using an Agilent Cary 630 FTIR spectrometer equipped with an attenuated total reflectance (ATR) accessory. Sixteen spectra were collected per sample to obtain an averaged spectrum over the frequency range of 450 – 4000 cm^{-1} with a resolution of 2 cm^{-1}.

X-ray photoelectron spectroscopy (XPS) analyses were performed using a Thermo Scientific K-Alpha X-ray photoelectron spectrometer equipped with an MXR3 Al Kα monochromatic X-ray source (hν = 1486.6 eV) and an X-ray gun set to 72 W (6 mA and 12 kV). All samples were ground in an agate mortar prior to analysis and individually mounted onto carbon tape. Thermo Avantage software allowed processing the data for B 1*s*, N 1*s*, O 1*s* and C 1*s* spectra. The adventitious carbon (C-C) peak set at 284.8 eV was used for binding energy calibration.

Near edge X-ray absorption fine structure (NEXAFS) spectroscopy experiments were carried out at the B07 beam line of Diamond Light Source, UK.[25] Samples were ground as powders and were mounted onto carbon tape. We used 400 lines per mm Pt gratings of the beamline's

plane grating monochromator with an exit slit width of 50 μm, which leads to an energy resolution of 50 meV and 200 meV at the B and O K-edge, respectively. B K-edge and O K-edge spectra were recorded at room temperature under ultra-high vacuum (UHV, typically 10^{-8} mbar) on INT-600, INT-800 and final porous BN referenced as BN-1050-$t_{3.5}$.

Solid-state ^{11}B nuclear magnetic resonance (NMR) spectra were recorded using a Bruker Avance III spectrometer equipped with a wide-bore 14.1 T superconducting magnet (^{11}B Larmor frequency of 192.6 MHz) and a Bruker 4-mm BN-free magic angle spinning (MAS) probehead. Samples were ground and packed into zirconia rotors, which were rotated about an axis inclined at the magic angle at a rate of 10 kHz. Spectra were acquired using a single soft pulse ($\nu_1 \approx 20$ kHz) of short flip angle ($\beta \approx 7°$) to enable quantitation of signals with widely different magnitudes of the quadrupolar coupling constant (C_Q). For the INT-RT and INT-100 samples, signal averaging was carried out for 128 transients with a recycle interval of 2 s, whereas T_1 relaxation was observed to be slower for all other samples and signal averaging for those was carried out for 64 transients with a recycle interval of 30 s. All spectra were recorded with high-power ($\nu_1 \approx 90$ kHz) continuous wave decoupling of ^{1}H during acquisition, to improve the resolution of signals for any protonated species. Chemical shifts are reported relative to $BF_3.Et_2O$ using BPO_4 ($\delta = -3.3$ ppm) as a secondary solid reference. The ^{11}B multiple-quantum (MQ) MAS spectra of selected samples were recorded using a z-filtered amplitude-modulated pulse sequence, with signal averaging for 24 or 120 transients for each of 90 t_1 increments of 50 μs. Spectra are shown after shearing and referencing in δ_1 according to the formalism of Pike et al.[26]

Density functional theory (DFT) calculations were carried out at the B3LYP/6-311+G(2d,p) theory level using GAUSSIAN 09 revision D.01.[27] Calculations were performed on an individual 32-core Intel Broadwell nodes of the University of St Andrews computing cluster. Computed magnetic shieldings (σ_{iso}) were converted to computed chemical shifts (δ_{iso}) using

$\delta_{iso} = \sigma_{ref} - \sigma_{iso}$, with a value of σ_{ref} = 100.0038 ppm determined using $BF_3.Et_2O$ (calculated at the same theory level).

Solid-state ^{13}C NMR spectra were recorded using a Bruker Avance III spectrometer equipped with a wide-bore 9.4 T superconducting magnet (^{13}C Larmor frequency of 100.9 MHz). Samples were packed into standard 4 mm ZrO_2 rotors and rotated about an axis inclined at the magic angle at a rate of 12.5 kHz. Spectra were recorded with direct polarisation using a rotor-synchronised spin-echo pulse sequence (τ = 80 μs) to eliminate the probe background. Signal averaging was carried out for either 640 transients (INT-600, C_3N_4) or 1024 transients (INT-RT, INT-200) with a recycle interval of 90 s. Spectra were processed with 20 Hz exponential broadening. Chemical shifts are reported in ppm relative to TMS using the CH_3 signal of L-alanine (δ = 20.5 ppm) as a secondary solid reference.

2.2.2 Structural features of porous BN and its reaction intermediates

Powder X-ray diffraction (XRD) in reflection mode was carried out using a PANalytical X'Pert Pro X-ray diffractometer with an anode voltage of 40 kV and an emission current of 20 mA using a monochromatic Cu Kα radiation (λ = 1.54178 Å). The XRD detector was a silicon strip detector X'Celerator. All samples were ground prior to measurement.

Nitrogen sorption isotherms were collected with a Micromeritics 3Flex porosity analyser at –196 °C. All samples were first degassed overnight at 140 °C and 0.2 mbar and then degassed in-situ at 120 °C for 4 h at 0.0030 mbar. Specific surface area was evaluated with the Brunauer-Emmett-Teller (BET) method.[28] The total pore volume was estimated from the volume of N_2 adsorbed at a relative pressure P/P_0 of 0.97. The micropore volume was determined using the Dubinin-Radushkevich method.[29]

2.2.3 Thermal decomposition pathways of the precursors and reaction intermediates

Thermogravimetric analysis coupled with mass spectrometry (TGA: Netzsch TG 209 F1 Libra; MS: Netzsch QMS 403 D Aëolos) was used for the initial mixtures of reagents with one or two N-precursors: boric acid and melamine (BA:M; molar ratio 1:1); boric acid and urea (BA:U; molar ratio 1:5) and the three precursors combined (BA:M:U; molar ratios 1:1:5). Prior to measurement, the mixtures were finely ground in an agate mortar for 3 min to mimic the preparation process used before synthesis in the furnace. This technique enabled study of the mass loss during synthesis and the corresponding gases released during heating up to 1050 °C with a ramp of 10 °C min^{-1}. To investigate the individual roles of urea and melamine as N-precursors, porous BN obtained after TG analysis was collected for further characterisation.

3. Results & Discussion

3.1 Chemical aspects of the formation of porous BN

We obtained consistent results for the final porous BN product in terms of macroscopic appearance (Figure 1a) and chemical composition (Figures 2, 3) compared to porous BN synthesised following the same methodology.[11, 24] All the intermediates were collected after synthesis in the furnace and were analysed to investigate their composition and understand the chemical formation of porous BN. INT-RT and INT-100 were powders whereas the samples prepared at 200 °C and above appeared as flakes (Figure 1a). Two intermediates were distinct by their yellow colour: INT-600 and INT-700 (Figure 1a). This unique characteristic suggests important implications and will be discussed later alongside the characterisation results.

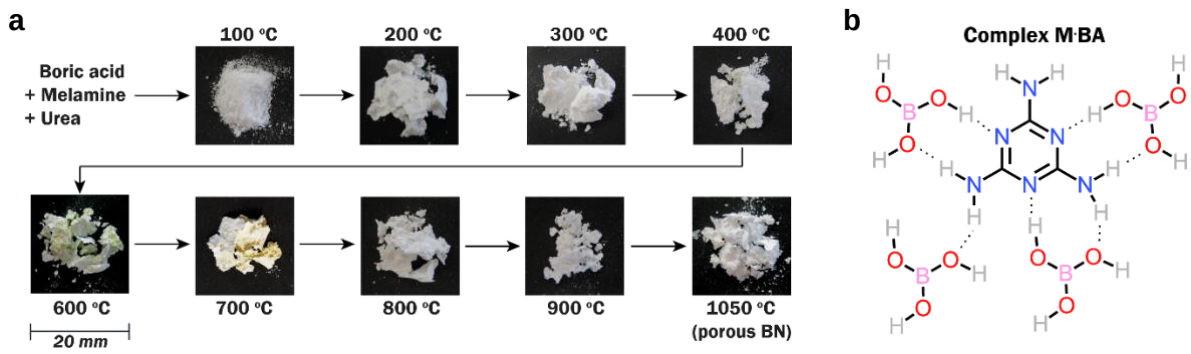

Figure 1. (a) Macroscopic aspect of the reaction intermediates and final product porous BN. (b) Chemical structure of the adduct M·BA formed by melamine and boric acid via hydrogen bonding.

Starting intermediate, room temperature – We now focus on the chemical features of the intermediates. We first recorded the FTIR spectra for each reagent individually (Figure S1a) to calculate the expected spectrum of the mixture without any interaction by considering the relative amounts of reagents. To identify IR bands and assess the interaction between the initial reagents upon mixing, we compared the calculated FTIR spectrum with the experimental spectrum of INT-RT (Figure S1b and Figure 2a). Boric acid was not traced at RT due to its low quantity in the initial mixture compared to the N-containing precursors. This was confirmed by the calculated FTIR spectrum based on the initial composition. However, we observed differences between the expected FTIR spectrum and the one obtained, especially in the 3100 – 3470 cm^{-1} region corresponding to OH and NH_2 groups. INT-RT exhibited bands at 3469, 3426, 3326 cm^{-1} accounting for NH_2 groups of melamine and urea, whereas the calculated spectrum only showed bands at 3418 and 3323 cm^{-1} (Figure S1b). The presence of an additional band at higher frequency, 3469 cm^{-1}, and the redshift of the two other bands could be linked to hydrogen bonding (H bonding) between melamine and boric acid.[30] We attributed the 3256 cm^{-1} band observed in both INT-RT and the calculated spectrum to NH_2 groups from urea, which appeared unaffected by hydrogen bonding. From this observation, we hypothesised that boric acid and melamine formed a melamine-boric acid adduct (M·BA) via H bonding after

mechanical mixing at RT (Figure 1b). The proportion of this adduct in the sample is not known and pristine reagents are likely to still be present in significant quantity, which might be the reason why no signs of this intermediate are observed on the XRD patterns. Previous studies showed that M·BA adducts adopt a specific configuration with only two amino groups from melamine involved in H bonding with three to four boric acid molecules.[30, 31] This adduct explains the additional IR band observed at 3469 cm^{-1} in INT-RT corresponding to the different N-H bond length when NH_2 groups from melamine molecules are involved in H bonding. The two red-shifted bands at 3418 and 3323 cm^{-1} correspond to NH_2 groups not contributing to H bonding but affected by a different chemical environment.

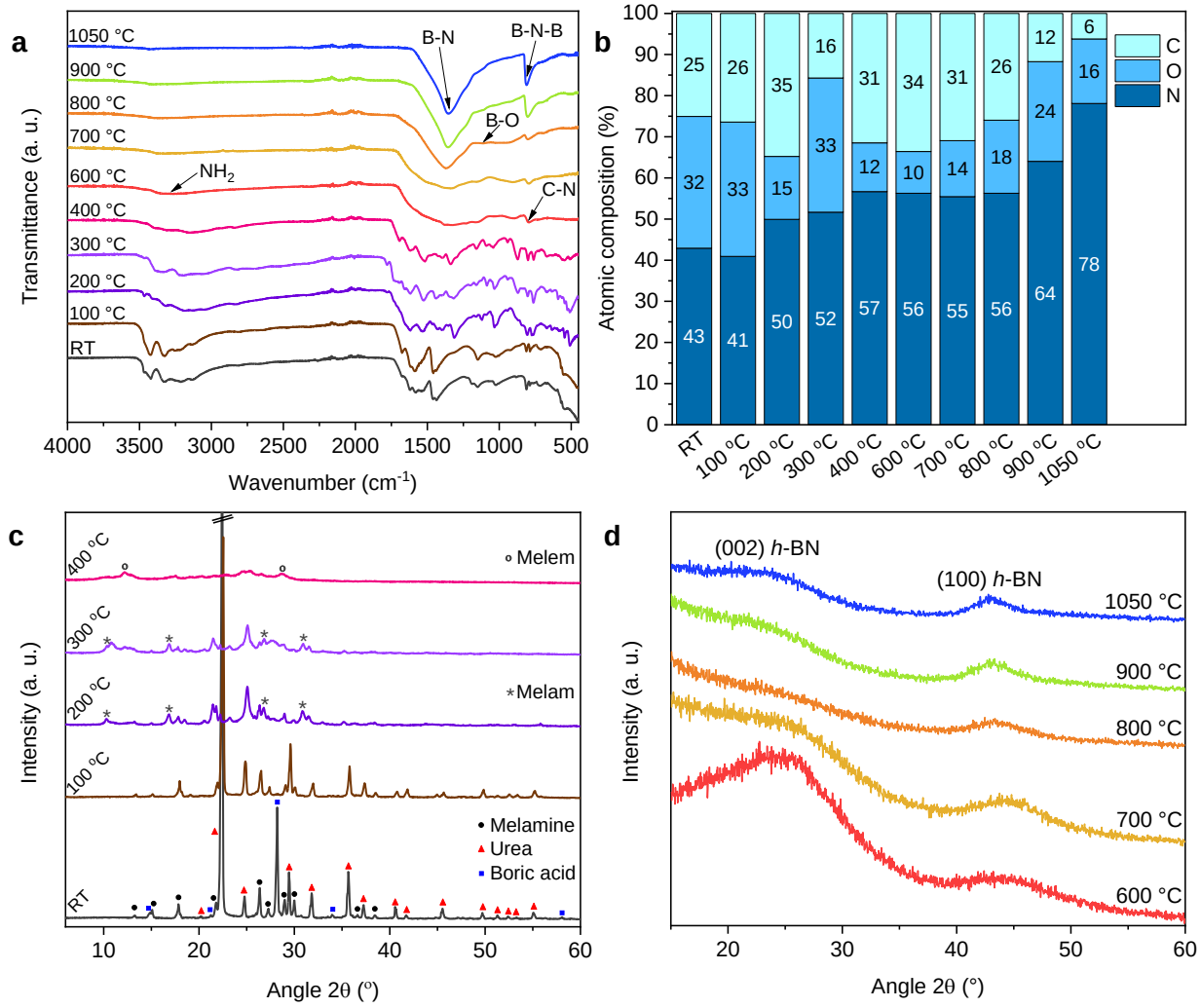

Figure 2. (a) FTIR spectra for all the intermediates. (b) Estimated atomic composition derived from XPS. The data were normalised based on the constant boron content. (c) XRD profiles for the intermediates obtained between 100 and 400 °C. (d) XRD profiles for the intermediates obtained between 600 and 1050 °C (note: a different vertical scale is used for clarity).

Between room temperature and 100 °C – Here, we observed a minor change in composition based on the FTIR and XPS analyses (Figures 2a, 2b, 3). We note that the atomic composition derived from XPS measurements in Figure 2b is normalised to the boron content, which remains constant during the synthesis due to its thermal stability (boron's melting point is 2077 ºC). The initial composition exhibited lower %N and higher %O than expected from a theoretical calculation based on the amounts of precursors (Table S1). This variation appears as XPS, a surface-sensitive technique, provided only the surface composition. The formation of the M·BA adduct can likely modify the surface composition after grinding at RT. In the XRD patterns, we observed the three precursors at RT (Figure 2c, see reagents XRD patterns in Figure S1c). INT-100 exhibited the same XRD peaks as INT-RT corresponding to urea (e.g., 22, 25, 29, 32 and 36°) and melamine (e.g., 18, 22, 26, 29 and 30°), but with lower intensities, and the boric acid peaks were not present (Figure 2c). These changes could indicate the conversion of boric acid into boron oxide (B_2O_3) with the release of water,[32] and/or the formation of another B-containing species. Indeed, quantitative ^{11}B NMR spectra confirm that a large portion (~72%) of the B is trigonal in INT-100, as expected for either $B(OH)_3$ or B_2O_3 (Figure 4a). However, the remaining 28% of the B spectral intensity corresponds to tetrahedral species with isotropic shifts of 1.5 and 0.5 ppm. We hypothesise that these tetrahedral species correspond to adducts formed between boric acid and the amine groups present in urea and melamine. This is supported by the Lewis acid nature of boron and the Lewis basic nature of the amines.

Between 100 and 200 °C – The B 1*s* XPS peak corresponding to B-O bonds (192.9 eV) was replaced by a peak corresponding to B=O bonds (191.6 eV), showing that a significant quantity

of boric acid disappeared as it formed boron oxide (Figure 3a). Urea was mostly degraded at 200 °C, as shown by the disappearance of the corresponding signals in FTIR (e.g., C=O, 1677 cm^{-1} and C-N, 1457 cm^{-1} in Figure 2a) and XRD (e.g., 22, 29, 36° in Figure 2c). Urea decomposed into sub-products such as biuret, cyanuric acid and ammelide, which can coexist over a wide range of temperatures.[33, 34]

Between 200 and 400 °C – At 200 °C, a new FTIR band was observed at 1311 cm^{-1}, which shifted towards higher wavenumbers at 300 °C and 400 °C. We identified this band as melam, which is one of the condensates of melamine with two bonded triazine rings.[35] We attributed the gradual shift to 1343 cm^{-1} at 400 °C to a further condensation into melem, containing a tri-s-triazine ring.[35, 36] Additionally, the band at 809 cm^{-1} in INT-200 is characteristic of the triazine ring of melamine and melam whereas the band at 798 cm^{-1} in INT-300 and INT-400 is characteristic of the tri-s-triazine ring of melem.[37-39] The sharp band appearing at 874 cm^{-1} in INT-300 and INT-400 is also characteristic of the tri-s-triazine ring of melem.[38] In XRD, we observed peaks at 10°, 17°, 27° and 31° in INT-200 (Figure 2c). These four peaks remained at 300 °C with equal intensities but were not observed at 400 °C, which suggests the condensation of melamine and melam into melem at 400 °C. We attributed the new peaks at 12° and 28° in INT-400 to melem.[36] This was consistent with the XPS of INT-400 showing a new C 1*s* peak at a binding energy of 288.3 eV, corresponding to CN_3 environments present in melem. In parallel, the evolution of boric acid and urea likely contributed to an amorphous transition of the mixture, and no clear peaks were observed in XRD beyond 400 °C.

Over the 200-400 °C temperature range, the quantitative ^{11}B NMR spectra show that the vast majority of B is present in tetrahedral environments, giving rise to isotropic shifts of 0, –1.9 and –4.5 ppm (Figure 4a). Around 11-23% of B is trigonal, with peak positions consistent with BO_3 and, at 400 °C, BN_2O local environments (Figure S4). The tetrahedral species could

correspond to B atoms being coordinated to carbon/nitrogen-based structures evolving in the reaction medium.

Between 400 and 700 °C – 600 °C marked a crucial transition in the synthesis process: the product appeared yellow to the naked eye and was completely amorphous based on the broad XRD features (Figures 1a, 2d). INT-700 was also yellow and amorphous. The yellow colour of these samples suggested the presence of carbon nitride. [21, 36] We note that some IR bands of carbon nitride and BN compounds can overlap, e.g., bands at 812 cm^{-1}, 891 cm^{-1} and between 1200 and 1600 cm^{-1}.[40] This effect complicates the interpretation of the FTIR spectra for INT-600 and INT-700 (Figure 2a). Bearing that in mind, we did not clearly see the characteristic IR band for B-N bonds (~1354 cm^{-1}) in INT-600 and INT-700 (Figure 2a), suggesting that significant porous BN did not form at 600 °C nor 700 °C. The XRD patterns of INT-600 and INT-700 showed broad humps around 24° and 44°, which typically correspond to the (002) and (100) planes in graphitic-like structures, such as BN and C_3N_4.[37, 38, 40] Although matching with the profile of porous BN, the hump around 44° could also correspond to the tri-s-triazine ring observed in melem and carbon nitride.[38, 41] This suggestion is further supported for INT-600 by the rest of the pattern below 24° that differed from BN (Figure 2d). However, the XRD profile of INT-700 seemed to be intermediate between those of INT-600 and INT-800. We did not observe the characteristic B 1*s* peak for B-N bonds (191.2 eV) in the XPS of INT-600 whereas it started appearing in INT-700 (Figure 3a). The carbon content was still high in INT-700 but decreased significantly in INT-800, as observed in the estimated composition in XPS (Figure 2b). Based on the yellow colour of both INT-600 and INT-700 and the previous analyses, we propose the formation of carbon nitride prior to the formation of porous BN. INT-600 and INT-700 appeared amorphous and non-porous as discussed below. These observations supported the hypothesis that carbon nitride formed, since this material has low porosity.[42] Some BN was observed in INT-700, but in too little proportion to observe porosity. We discuss

this aspect further in section 3.2. ^{13}C NMR confirmed further the formation of carbon nitride in INT-600 (Figure S6). Condensation towards carbon nitride-like species, such as melam and melem, starts at relatively low temperature (~200 °C) but is not complete even by 600 °C (Figure S6).

The quantitative ^{11}B MAS NMR spectra of INT-600 and INT-700 (Figure 4a) show that the majority of B remains tetrahedral at this stage in the reaction (80% for INT-600, 75% for INT-700). However, in contrast to the sharp signals for the samples formed at 200-400 °C, the resonances at 600 and 700 °C are much broader, indicative of a loss of longer-range order (consistent with the XRD data, Figures 2c and 2d). While the signal for the tetrahedral B is essentially unchanged between 600 and 700 °C, what little trigonal B is present does change in environment, with the peak positions consistent with predominantly BO_3 and a smaller amount of BN_2O at 600 °C and almost exclusively BN_2O at 700 °C.

Between 700 and 1050 °C – BN formed between 700 and 800 °C, as supported by the B-N bonds identified in FTIR (1354 cm^{-1} for B-N and 812 cm^{-1} for B-N-B; Figure 2a)[43], in XPS (191.2 eV for B 1*s* and 398.6 eV for N 1*s*; Figures 3a and 3b)[44] and ^{11}B MAS NMR (for BN_3 environments; Figures 4a and c), as well as the (002) and (100) XRD humps (respectively 24° and 44°; Figure 2d) expected for amorphous BN.[18] On the FTIR spectra, B-O bands (~1120 cm^{-1}) gradually disappeared between 800 °C and 1050 °C (Figure 2a). In parallel, the content of carbon decreased as seen in XPS (Figure 2b). The dwell time of 3.5 h at 1050 °C did not significantly change the structure of porous BN as we obtained identical results for BN-1050-t_0 and BN-1050-$t_{3.5}$, but it contributed to further overall conversion into porous BN with a decrease in O and C impurities (Figures S2a and c). The ^{11}B MAS NMR spectra of the samples formed above 700 °C show a loss of tetrahedral B, with only ~1% B in a tetrahedral environment by 1050 °C (Figures 4a, 4b). For INT-800 and INT-900, some BO_3 signals are observed, although by 1050 °C, the trigonal B is almost exclusively in a BN_3 environment, as

would be expected in hexagonal BN, and only a trace (~7%) of BN_2O is observed for this sample.

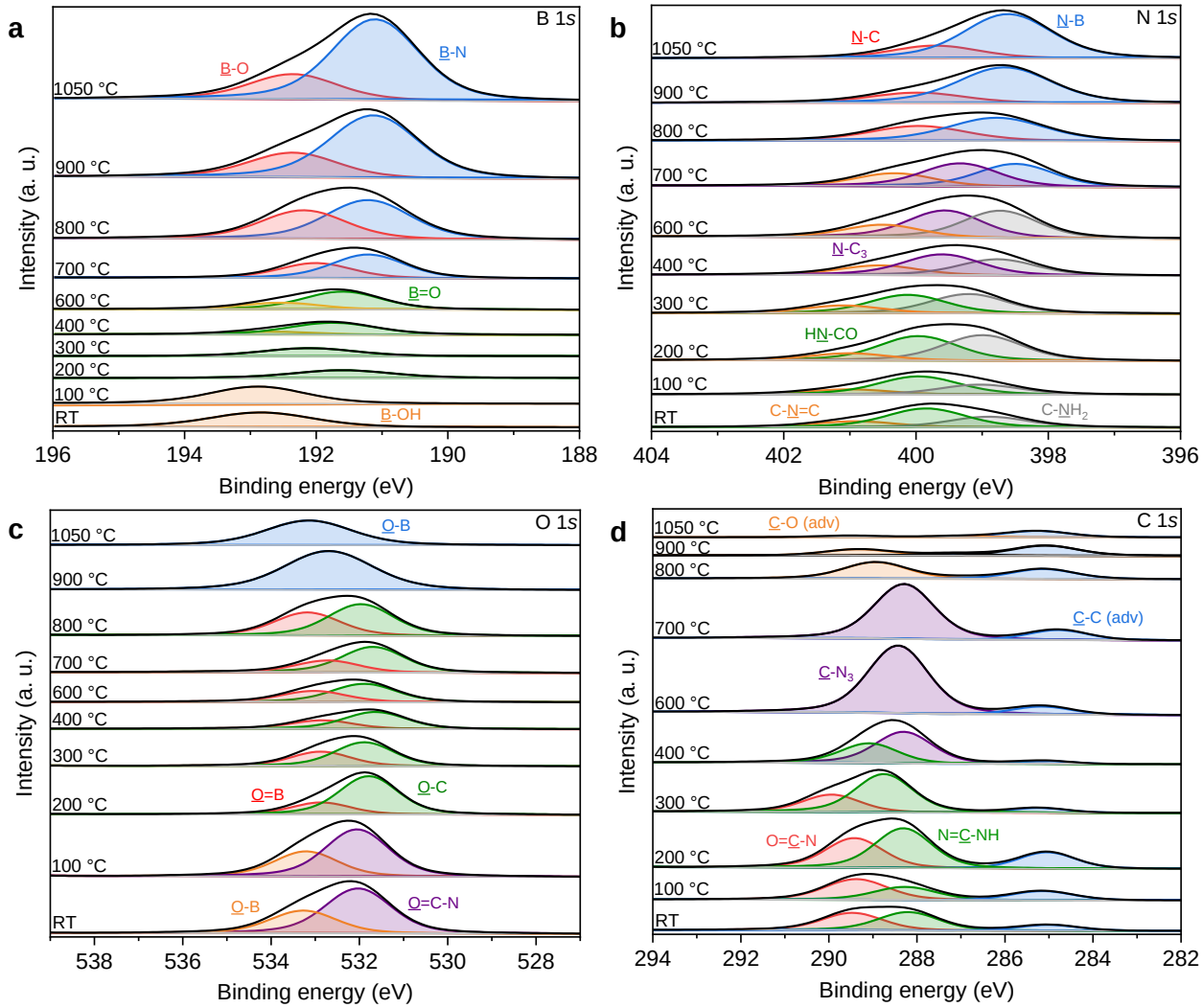

Figure 3. XPS peaks of (a) B 1*s* (b) N 1*s* (c) O 1*s* and (d) C 1*s* of all the intermediates.

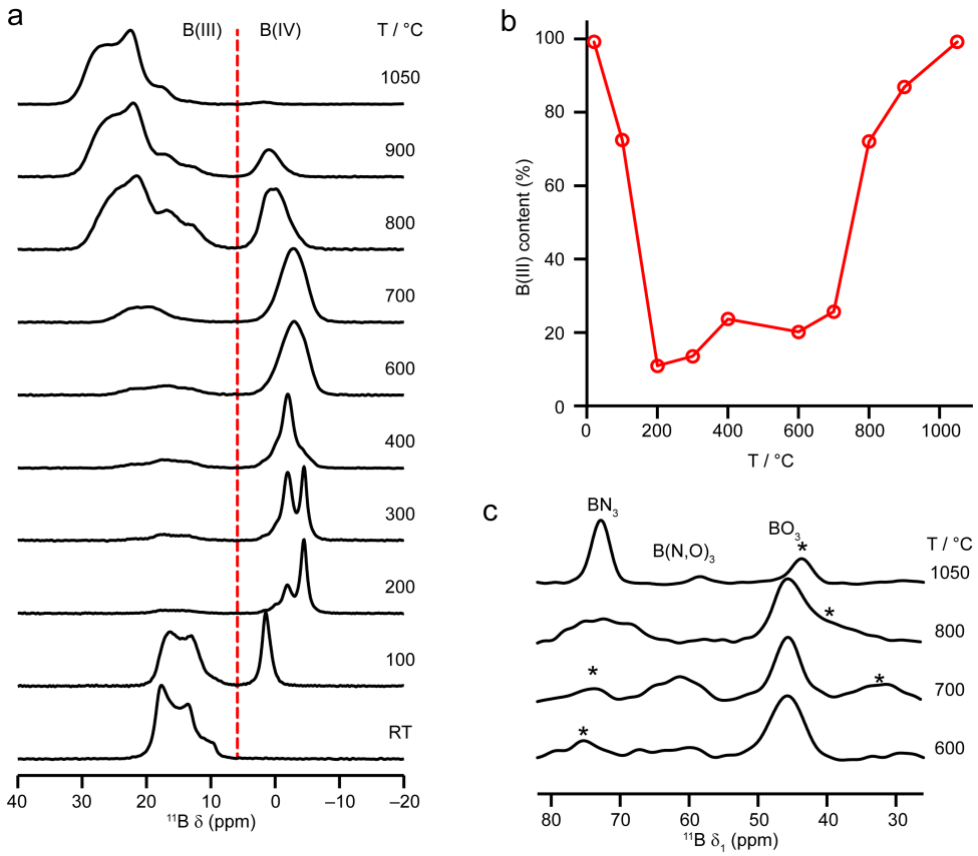

Figure 4. (a) $^{11}B\{^{1}H\}$ (14.1 T, 10 kHz MAS) NMR spectra of all of the intermediates. The dotted line at 6 ppm shows the border between trigonal (> 6 ppm) and tetrahedral (< 6 ppm) B signals. (b) The proportion of trigonal B signal determined from integrated intensities from the spectra in (a). (c) δ_1 projections of the trigonal B signals observed in ^{11}B MQMAS spectra for selected intermediates. Spinning sidebands are marked * (see Figure S3).

We then used NEXAFS to complement XPS and NMR and help identify varying chemical states and environments for B atoms. NEXAFS detects signals from π and σ* orbitals in the samples, where π bonding involving B atoms would indicate the presence of compounds containing B-O-N or B-N environments. The absence of π bonding would point towards boron oxide only, prior to the formation of porous BN. In the case of π bonding, the identification of B-O or B-N bonds would indicate the chemical environments of B atoms, shedding light on the advancement of the formation of porous BN. We tested three samples with B K-edge measurements to follow the formation of porous BN: INT-600, INT-800 and BN-1050-$t_{3.5}$ (Figure 5). Based on our previous results, we did not expect to observe BN patterns below 700

°C (Figures 2, 3, 4). Indeed, no π signal was observed for boron in INT-600, which confirmed that BN had not formed at 600 °C as carbon nitride would still be predominant (Figure 5). INT-800 exhibited four peaks, each corresponding to a different atomic environment for B atoms: BN_3, BN_2O, BNO_2 and BO_3 (see Figure 5 for visualisation). The BN_3 peak at 191.3 eV corresponds to the only peak that would be observed in pure hexagonal BN.[45] The doublet peak (198; 199 eV) is linked to the corresponding σ* transition.[46, 47] The three other π peaks represent defects where B atoms are bonded to one, two or three O atoms, confirming that the formation of porous BN is still ongoing at 800 °C. INT-1050-$t_{3.5}$ exhibited the same four π peaks but in different proportions: BN_3 was predominant compared to BN_2O, BNO_2 and BO_3, which we expect in porous BN where a lower content of O was measured in XPS (Figure 2b). The XPS results are corroborated by the ^{11}B MQMAS spectra of INT-600, INT-700, INT-800 and BN-1050-$t_{3.5}$ (δ_1 projections shown in Figure 4c, full spectra shown in the Supporting Information, Figure S3), which show that the majority of trigonal B is present in BN_3 environments (δ_1 = 69-79 ppm), but some BN_2O and BNO_2 (δ_1 = 60-65 ppm), and BO_3 (δ_1 = 44-46 ppm) are also present (see Supporting Information and Figure S4 for further details of the assignments).

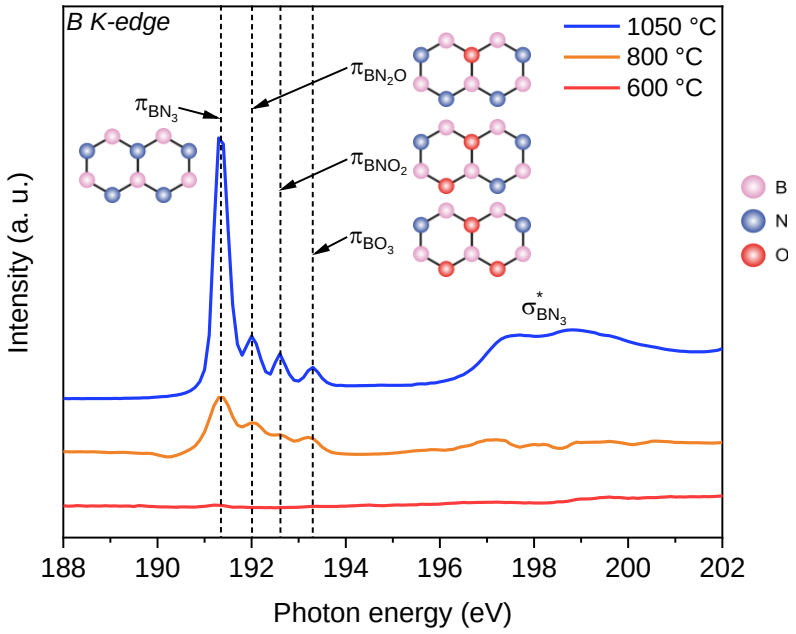

Figure 5. B K-edge NEXAFS for the intermediates at 600 °C, 800 °C and the final product BN-1050-$t_{3.5}$, with schematics of the different chemical environments for B atoms.

3.2 Porosity development during the formation of porous BN

Alongside the chemical formation of porous BN, we investigated its porosity development to understand how to tune the porosity depending on the targeted application. The final product, porous BN, typically shows a type IV isotherm with a type H3/H4 hysteresis loop, indicating the presence of slit-shaped micropores and mesopores. [48]

Based on the XRD patterns, we observed that the amorphous transition started from around 400 °C, with INT-600 and INT-700 being completely amorphous (Figure 2d). However, neither INT-600 nor INT-700 exhibited surface area or porosity using N_2 sorption at –196 °C (Figure 6). This aligns with the hypothesis that INT-600 and INT-700, despite being amorphous, were composed of carbon nitride whose porosity is typically under 100 $m^2\ g^{-1}$.[42] At 800 °C, the surface area dramatically increased to 1539 $m^2\ g^{-1}$ and the total pore volume reached 0.869 $cm^3\ g^{-1}$ with both micropores and mesopores derived from the type IV isotherm (Figure 6). The intermediate at 900 °C exhibited a slight decrease in surface area and micropore

volume, whereas the total pore volume slightly increased, implying higher macropore and mesopore volumes. The final temperature 1050 °C with dwell time (BN-1050-$t_{3.5}$) led to a surface area of 1616 m^2 g^{-1} and a total pore volume of 1.066 cm^3 g^{-1}. This 3.5 h dwell period did not significantly change the surface area nor the pore volume as BN-1050-t_0 had a surface area of 1664 m^2 g^{-1} and a total pore volume of 1.066 cm^3 g^{-1} (Figure S2e). However, XPS data suggests that the dwell period allowed further conversion into BN with a decrease in C and O content (Figure S2c). Choosing between a slightly higher purity or higher surface area would depend on the specific application that is required.

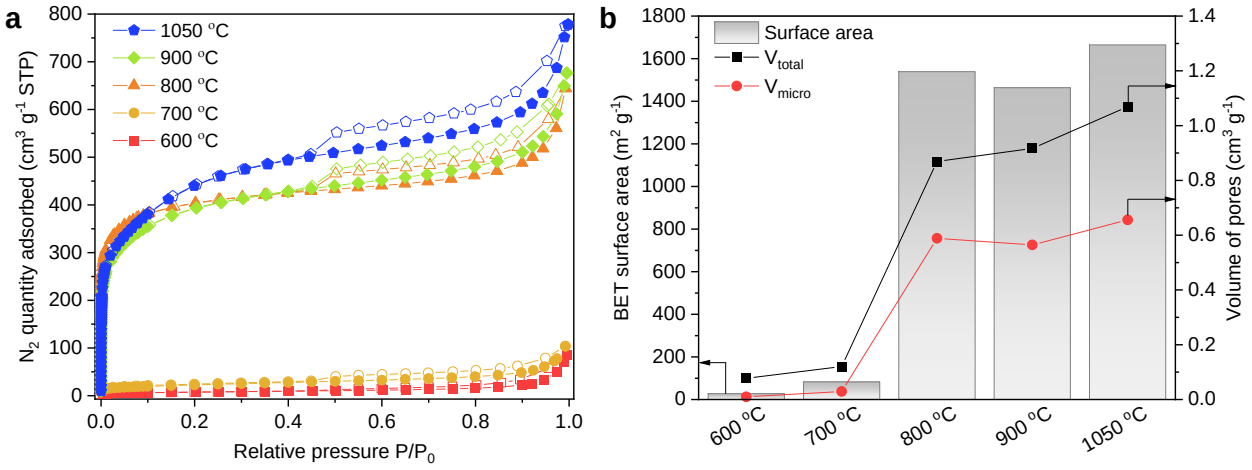

Figure 6. (a) N_2 sorption isotherms at –196 °C (full symbols = adsorption; open symbols = desorption) and (b) associated textural parameters for the intermediates synthesised at 600 °C and above.

Next, we conducted TG-MS analyses to assess the role of gas release in the formation of BN and the development of its porosity. Between 700-800 °C where porosity and surface area increased (Figure 6), the main gases released were CO_2 and HCN (Figure 7). This corresponds to the conversion to boron nitride via the reaction between carbon nitride and boron-containing

species. This was corroborated by the significant decrease in C observed in XPS analyses (Figure 2b). Therefore, CO_2 and HCN are the main porogens in the formation of porous BN.

Below 700-800 °C, we identified four steps of significant weight loss that echoed results obtained in 3.1. After moisture removal and NH_3 release (60-140 °C), we observed NH_3 and CO_2 release from urea degradation (160-230 °C) as well as N_2H_4 and HCN. Subsequently, NH_3, CH_2N_2, HCNO and CO_2 release (250-400 °C) occurred due to the decomposition of the urea sub-products, such as biuret, cyanuric acid, ammeline and ammelide,[34] and the condensation of melamine into melam and melem.[35, 36] Finally, we observed further release of NH_3 and CO_2 (450 °C to 625 °C) owing to similar decomposition and condensation reactions that lead to non-porous carbon nitride formation.[40] Above 800 °C, a quasi-plateau was observed in TGA, corresponding to the condensation of BN with minor release of O as shown in FTIR (Figure 2a), XPS (Figures 2b, 3c) and NEXAFS analyses (Figure 5).

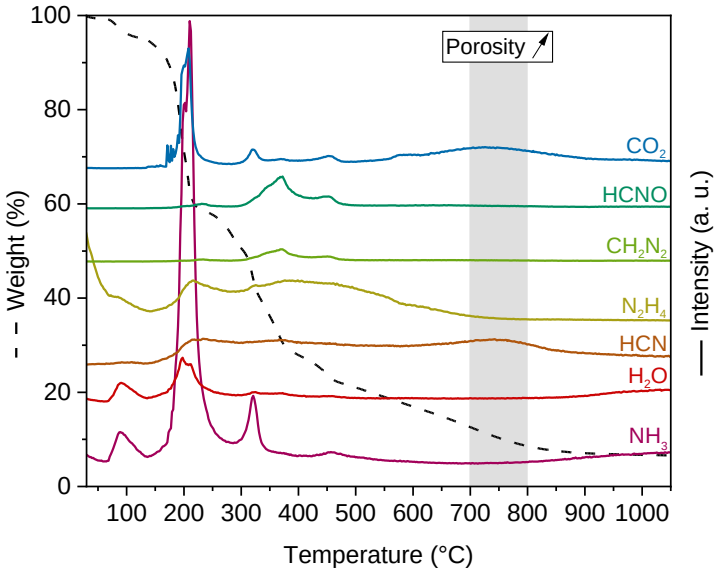

Figure 7. TG-MS in N_2 for the initial mixture of boric acid, melamine and urea. MS signals include: NH_3 (m/z = 17), H_2O (m/z = 18), HCN (m/z = 27), N_2H_4 (m/z = 32), CH_2N_2 (m/z = 42), HCNO (m/z = 43) and CO_2 (m/z = 44).

3.3 Formation mechanism of porous BN

Based on our interpretation of the characterisation analyses, we propose a formation mechanism of porous BN with boric acid, melamine and urea reacting under N_2 atmosphere up to 1050 °C (Figure 8). From RT to around 500 °C, the degradation of urea into biuret, cyanuric acid, ammelide, ammeline and eventually melamine took place. These decompositions led to significant weight loss and gas release (e.g., water and ammonia). Concurrently, we observed the condensation of melamine into melam and melem with the formation of tri-s-triazine rings. In parallel, boric acid was converted into B-containing species displaying either trigonal B (i.e., B_2O_3, $B(OH)_3$) or tetrahedral B (adducts formed between boric acid and the amine groups). Around 500 °C, melem evolved further to form carbon nitride clearly identified in the two yellow intermediates INT-600 and INT-700. Although the samples were amorphous at these temperatures, no porosity had developed. Thanks to the reaction of carbon nitride with boron-containing species, such as B_2O_3, X_2B-OH, X_2B=O, X_2B=N (where X = C or N) depending on the temperature, boron oxynitride BON was formed via the release of HCN and CO_2, identified as porogens in the synthesis. Porosity then developed between 700 and 800 °C via further release of HCN and CO_2 forming pores in the BON structure. As the temperature increased over 800 °C, O and C atoms evolved as CO_2 and H_2O to form porous BN. Some O impurities remained even at 1050 °C but in small quantities.

The mechanism above relates to the synthesis conditions we have explored in this study. Yet, we speculate that if using melamine and urea, a similar carbon nitride intermediate would form since heating melamine or urea eventually leads to carbon nitride. Overall, we assume the type of chemistry involved in the reactions would not change significantly, but the temperatures at which intermediates form could vary depending on the precursors (e.g., temperature at which NH_3 is generated, formation of carbon nitride etc.,).

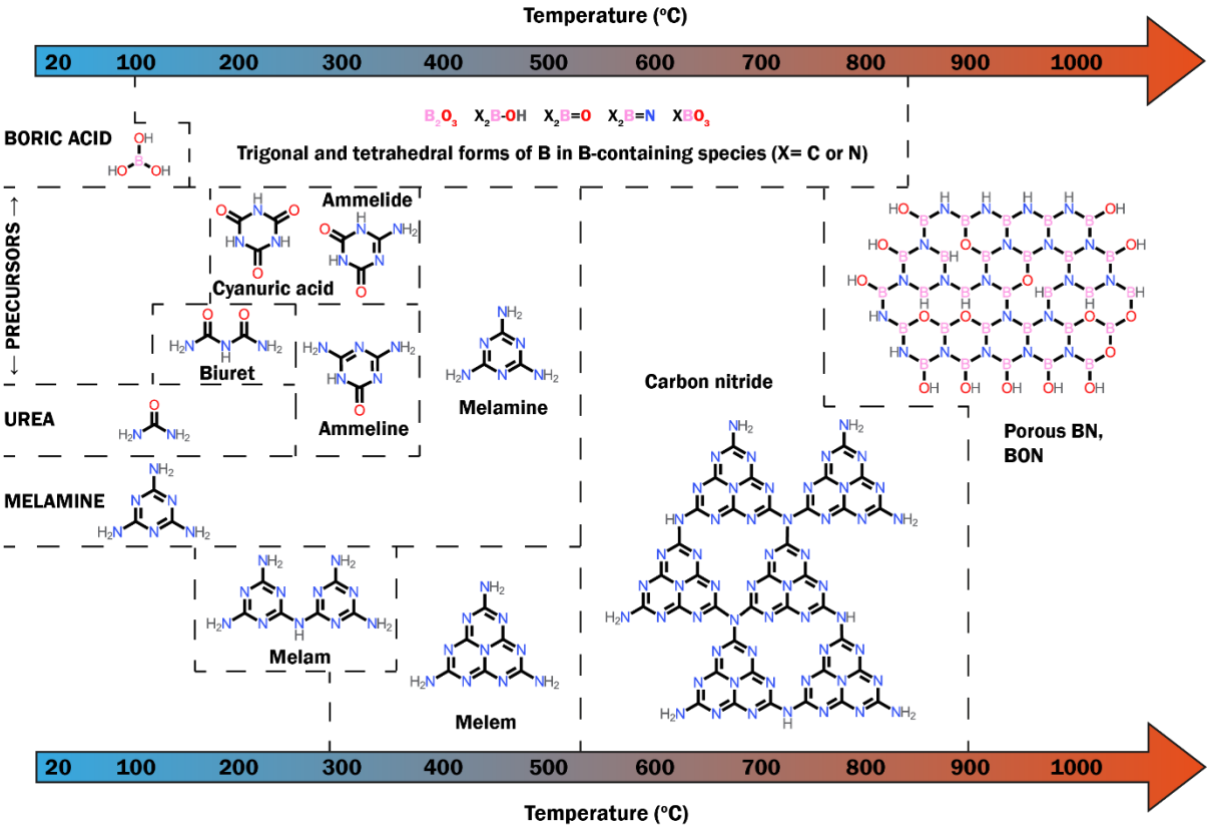

Figure 8. Proposed species evolution during the formation of porous BN from boric acid, melamine and urea under N_2 atmosphere up to 1050 °C.

4. Conclusions

We investigated the chemical formation and the porosity development of porous BN under a N_2 atmosphere with analytical and spectroscopic techniques. This allowed us to propose a formation mechanism highlighting the most critical stages of the synthesis for this specific synthesis parameter space. In particular, we found that porous BN formed only above 700 °C, with a dramatic increase in surface area between 700 and 800 °C. Up to 700 °C, various reaction intermediates were identified, including non-porous carbon nitride, which eventually reacted with a tetrahedral form of boron to form boron nitride. This study also showed that both urea and melamine, which act as chemical precursors and porogens, are crucial in the formation of

porous BN. These results bring further understanding on how porous BN is formed and shed light on how and when porosity develops, which is critical for industrial scale-up towards adsorption applications.

SUPPORTING INFORMATION

Additional chemical aspects of the reaction precursors (boric acid, melamine and urea) and carbon nitride. Comparison of porous BN obtained with and without final dwell time at 1050 °C. Additional ^{11}B solid-state NMR spectra and associated Density Functional Theory (DFT) calculations. ^{13}C solid-state NMR spectra from some intermediates and carbon nitride. Additional O-K edge NEXAFS results. FTIR and TG-MS results highlighting the roles of melamine and urea as N-precursors in the synthesis of porous BN.

ACKNOWLEDGMENT

The authors thank Patricia Carry and Kaho Cheung for the use and support of the Analytical Laboratory in the Department of Chemical Engineering at Imperial College London, and Gwilherm Kerherve for the use and support of the XPS suite in the Department of Materials at Imperial College London. The authors would also like to thank Leslie Bolton, Mark Sankey, Mandar Thakare, Sheetal Handa and Aldo Guiducci for the technical support with the bp-International Centre for Advanced Materials (bp-ICAM). This work was carried out with the support of Diamond Light Source, instrument B07 (proposal SI-26588). We acknowledge the funding from bp-ICAM and the funding from the Engineering and Physical Sciences Research Council (EPSRC) through the CDT in Advanced Characterisation of Materials (2018 NPIF grant EP/S515085/1).

REFERENCES

1. Marchesini, S.; Regoutz, A.; Payne, D.; Petit, C. Tunable Porous Boron Nitride: Investigating Its Formation and Its Application for Gas Adsorption. *Microporous Mesoporous Mater.* **2017,** *243*, 154-163.
2. Lei, W.; Portehault, D.; Liu, D.; Qin, S.; Chen, Y. Porous Boron Nitride Nanosheets for Effective Water Cleaning. *Nat. Commun.* **2013,** *4*, 1777.
3. Li, J.; Lin, J.; Xu, X.; Zhang, X.; Xue, Y.; Mi, J.; Mo, Z.; Fan, Y.; Hu, L.; Yang, X.; et al. Porous Boron Nitride with a High Surface Area: Hydrogen Storage and Water Treatment. *Nanotechnology* **2013,** *24*, 155603.
4. Wang, D.; Xue, Y.; Wang, C.; Ji, J.; Zhou, Z.; Tang, C. Improved Capture of Carbon Dioxide and Methane Via Adding Micropores within Porous Boron Nitride Fibers. *J. Mater. Sci.* **2019,** *54*, 10168-10178.
5. Xiao, F.; Chen, Z.; Casillas, G.; Richardson, C.; Li, H.; Huang, Z. Controllable Synthesis of Few-Layered and Hierarchically Porous Boron Nitride Nanosheets. *Chem. Commun.* **2016,** *52*, 3911-3914.
6. Maleki, M.; Beitollahi, A.; Shokouhimehr, M. Simple Synthesis of Two-Dimensional Micro/Mesoporous Boron Nitride. *Eur. J. Inorg. Chem.* **2015,** *2015*, 2478-2485.
7. Saha, D.; Orkoulas, G.; Yohannan, S.; Ho, H. C.; Cakmak, E.; Chen, J.; Ozcan, S. Nanoporous Boron Nitride as Exceptionally Thermally Stable Adsorbent: Role in Efficient Separation of Light Hydrocarbons. *ACS Appl. Mater. Interfaces* **2017,** *9*, 14506-14517.
8. Janik, J. F.; Ackerman, W. C.; Paine, R. T.; Hua, D.-W.; Maskara, A.; Smith, D. M. Boron Nitride as a Selective Gas Adsorbent. *Langmuir* **1994,** *10*, 514-518.
9. Shankar, R.; Sachs, M.; Francàs, L.; Lubert-Perquel, D.; Kerherve, G.; Regoutz, A.; Petit, C., Porous Boron Nitride for Combined CO_2 Capture and Photoreduction. *J. Mater. Chem. A* **2019,** *7*, 23931-23940.
10. Weng, Q.; Kvashnin, D. G.; Wang, X.; Cretu, O.; Yang, Y.; Zhou, M.; Zhang, C.; Tang, D.-M.; Sorokin, P. B.; Bando, Y.; et al. Tuning of the Optical, Electronic, and Magnetic Properties of Boron Nitride Nanosheets with Oxygen Doping and Functionalization. *Adv. Mater.* **2017,** *29*, 1700695.
11. Marchesini, S.; McGilvery, C. M.; Bailey, J.; Petit, C. Template-Free Synthesis of Highly Porous Boron Nitride: Insights into Pore Network Design and Impact on Gas Sorption. *ACS Nano* **2017,** *11*, 10003-10011.
12. Jiang, X.-F.; Weng, Q.; Wang, X.-B.; Li, X.; Zhang, J.; Golberg, D.; Bando, Y. Recent Progress on Fabrications and Applications of Boron Nitride Nanomaterials: A Review. *J. Mater. Sci. Technol.* **2015,** *31*, 589-598.
13. Marchesini, S.; Wang, X.; Petit, C. Porous Boron Nitride Materials: Influence of Structure, Chemistry and Stability on the Adsorption of Organics. *Front. Chem.* **2019,** *7*, 160.
14. Brožek, V.; Hubáček, M. A Contribution to the Crystallochemistry of Boron Nitride. *J. Solid State Chem.* **1992,** *100*, 120-129.
15. Ramirez Leyva, J. H.; Vitale, G.; Hethnawi, A.; Hassan, A.; Perez-Zurita, M. J.; Ruiz-Esparza, G. U.; Nassar, N. N. Mechanism of Hierarchical Porosity Development in Hexagonal Boron Nitride Nanocrystalline Microstructures for Biomedical and Industrial Applications. *ACS Appl. Nano Mater.* **2018,** *1*, 4491-4501.
16. Wu, C.; Wang, B.; Wu, N.; Han, C.; Zhang, X.; Shen, S.; Tian, Q.; Qin, C.; Li, P.; Wang, Y. Molecular-Scale Understanding on the Structure Evolution from Melamine Diborate Supramolecule to Boron Nitride Fibers. *Ceram. Int.* **2020,** *46*, 1083-1090.

17. Tian, T.; Hou, J.; Ansari, H.; Xiong, Y.; L'Hermitte, A.; Danaci, D.; Pini, R.; Petit, C. Mechanically Stable Structured Porous Boron Nitride with High Volumetric Adsorption Capacity. *J. Mater. Chem. A* **2021,** *9*, 13366-13373.
18. Alkoy, S.; Toy, C.; Gönül, T.; Tekin, A. Crystallization Behavior and Characterization of Turbostratic Boron Nitride. *J. Eur. Ceram. Soc.* **1997,** *17*, 1415-1422.
19. Postole, G.; Caldararu, M.; Bonnetot, B.; Auroux, A. Characterization of High Surface Area Hexagonal Boron Nitride by in Situ Electrical Conductivity. *Diamond Relat. Mater.* **2009,** *18*, 1052-1056.
20. O'Connor, T. E. Synthesis of Boron Nitride. *J. Am. Chem. Soc.* **1962,** *84*, 1753-1754.
21. Hoffendahl, C.; Duquesne, S.; Fontaine, G.; Bourbigot, S. Decomposition Mechanism of Melamine Borate in Pyrolytic and Thermo-Oxidative Conditions. *Thermochim. Acta* **2014,** *590*, 73-83.
22. Gong, Y.; Shi, G.; Zhang, Z.; Zhou, W.; Jung, J.; Gao, W.; Ma, L.; Yang, Y.; Yang, S.; You, G.; et al. Direct Chemical Conversion of Graphene to Boron- and Nitrogen- and Carbon-Containing Atomic Layers. *Nat. Commun.* **2014,** *5*, 3193.
23. Gross, P.; Höppe, H. A. Unravelling the Urea-Route to Boron Nitride: Synthesis and Characterization of the Crucial Reaction Intermediate Ammonium Bis(Biureto)Borate. *Chem. Mat.* **2019,** *31*, 8052-8061.
24. Shankar, R.; Marchesini, S.; Petit, C. Enhanced Hydrolytic Stability of Porous Boron Nitride Via the Control of Crystallinity, Porosity, and Chemical Composition. *J. Phys. Chem. C* **2019,** *123*, 4282-4290.
25. Held, G.; Venturini, F.; Grinter, D.; Ferrer, P.; Arrigo, R.; Deacon, L.; Garzon, W.; Roy, K.; Large, A.; Stephens, C.; et al. Ambient-Pressure Endstation of the Versatile Soft X-Ray (Versox) Beamline at Diamond Light Source. *J. Synchrotron Radiat.* **2020,** *27*.
26. Pike, K. J.; Malde, R. P.; Ashbrook, S. E.; McManus, J.; Wimperis, S. Multiple-Quantum Mas Nmr of Quadrupolar Nuclei. Do Five-, Seven- and Nine-Quantum Experiments Yield Higher Resolution Than the Three-Quantum Experiment? *Solid State Nucl. Magn. Reson.* **2000,** *16*, 203-215.
27. Frisch, M. J.; Trucks, G. W.; Schlegel, H. B.; Scuseria, G. E.; Robb, M. A.; Cheeseman, J. R.; Scalmani, G.; Barone, V.; Mennucci, B.; Petersson, G. A.; et al. *Gaussian 09*, Revision D.01; Gaussian, Inc.: Wallingford, CT, 2013.
28. Brunauer, S.; Emmett, P. H.; Teller, E. Adsorption of Gases in Multimolecular Layers. *J. Am. Chem. Soc.* **1938,** *60*, 309-319.
29. Chen, S. G.; Yang, R. T. Theoretical Basis for the Potential Theory Adsorption Isotherms. The Dubinin-Radushkevich and Dubinin-Astakhov Equations. *Langmuir,* **1994,** 10**,** 4244-4249.
30. Panicker, C. Y.; Varghese, H. T.; John, A.; Philip, D.; Nogueira, H. I. S. Vibrational Spectra of Melamine Diborate, $C_3N_6H_{62}H_3BO_3$. *Spectrochim. Acta, Part A* **2002,** *58*, 1545-1551.
31. Roy, A.; Choudhury, A.; Rao, C. N. R. Supramolecular Hydrogen-Bonded Structure of a 1:2 Adduct of Melamine with Boric Acid. *J. Mol. Struct.* **2002,** *613*, 61-66.
32. Randall, S. P.; Margrave, J. L. Vapour Equilibria in the B_2O_3-H_2O System at Elevated Temperatures. *J. Inorg. Nucl. Chem.* **1960,** *16*, 29-35.
33. Kinoshita, H. Synthesis of Melamine from Urea. *Rev. Phys. Chem. Jpn.* **1955,** *24*, 19-27.
34. Schaber, P. M.; Colson, J.; Higgins, S.; Thielen, D.; Anspach, B.; Brauer, J. Thermal Decomposition (Pyrolysis) of Urea in an Open Reaction Vessel. *Thermochim. Acta* **2004,** *424*, 131-142.

35. Wirnhier, E.; Mesch, M. B.; Senker, J.; Schnick, W. Formation and Characterization of Melam, Melam Hydrate, and a Melam–Melem Adduct. *Chem. – Eur. J.* **2013,** *19*, 2041-2049.
36. Jürgens, B.; Irran, E.; Senker, J.; Kroll, P.; Müller, H.; Schnick, W. Melem (2,5,8-Triamino-Tri-S-Triazine), an Important Intermediate During Condensation of Melamine Rings to Graphitic Carbon Nitride: Synthesis, Structure Determination by X-Ray Powder Diffractometry, Solid-State NMR, and Theoretical Studies. *J. Am. Chem. Soc.* **2003,** *125*, 10288-10300.
37. Wei, X.; Qiu, Y.; Duan, W.; Liu, Z. Cathodic and Anodic Photocurrents Generation from Melem and Its Derivatives. *RSC Adv.* **2015,** *5*, 26675-26679.
38. Xiong, Q.; Yuan, Y.; Zhang, L.; Xing, J.; Utama, M.; Lu, X.; Du, K.; Li, Y.; Hu, X.; Wang, S.; Genç, A.; Dunin-Borkowski, R.; Arbiol, J. High-Yield Synthesis and Optical Properties of G-C3n4. *Nanoscale* **2015,** *7*, 12343-12350.
39. Finkel'shtein, A. I.; Spiridonova, N. V. Chemical Properties and Molecular Structure of Derivatives of Sym-Heptazine[1,3,4,6,7,9,9b-Heptaazaphenalene, Tri-1,3,5-Triazine] *Russ. Chem. Rev.* **1964,** *33*, 400-405.
40. Liu, J.; Zhang, T.; Wang, Z.; Dawson, G.; Chen, W. Simple Pyrolysis of Urea into Graphitic Carbon Nitride with Recyclable Adsorption and Photocatalytic Activity. *J. Mater. Chem.* **2011,** *21*, 14398-14401.
41. Thomas, A.; Fischer, A.; Goettmann, F.; Antonietti, M.; Müller, J.-O.; Schlögl, R.; Carlsson, J. Cheminform Abstract: Graphitic Carbon Nitride Materials: Variation of Structure and Morphology and Their Use as Metal-Free Catalysts. *J. Mater. Chem.* **2008,** *40*, 4893-4908.
42. Wang, C.; Fan, H.; Ren, X.; Fang, J.; Ma, J.; Zhao, N. Porous Graphitic Carbon Nitride Nanosheets by Pre-Polymerization for Enhanced Photocatalysis. *Mater. Charact.* **2018,** *139*, 89-99.
43. Geick, R.; Perry, C. H.; Rupprecht, G. Normal Modes in Hexagonal Boron Nitride. *Phys. Rev.* **1966,** *146*, 543-547.
44. Cholet, V.; Vandenbulcke, L.; Rouan, J. P.; Baillif, P.; Erre, R. Characterization of Boron Nitride Films Deposited from BCl_3-NH_3-H_2 Mixtures in Chemical Vapour Infiltration Conditions. *J. Mater. Sci.* **1994,** *29*, 1417-1435.
45. Jiménez, I.; Jankowski, A. F.; Terminello, L. J.; Sutherland, D. G. J.; Carlisle, J. A.; Doll, G. L.; Tong, W. M.; Shuh, D. K.; Himpsel, F. J. Core-Level Photoabsorption Study of Defects and Metastable Bonding Configurations in Boron Nitride. *Phys. Rev. B* **1997,** *55*, 12025-12037.
46. Liu, L.; Sham, T.-K.; Han, W.; Zhi, C.; Bando, Y. X-Ray Excited Optical Luminescence from Hexagonal Boron Nitride Nanotubes: Electronic Structures and the Role of Oxygen Impurities. *ACS Nano* **2011,** *5*, 631-639.
47. Zhou, X. T.; Sham, T. K.; Chan, C. Y.; Zhang, W. J.; Bello, I.; Lee, S. T.; Heigl, F.; Jürgenen, A.; Hofsäss, H. Preferable Orientation of Turbostratic BN Basal Planes from an X-Ray Absorption Study. *J. Mater. Res.* **2006,** *21*, 147-152.
48. Sing, K. S. W.; Everett, D. H.; Haul, R. A. W.; Moscou, L.; Pierotti, R. A.; Rouquerol, J.; Siemieniewska, T. Reporting physisorption data for gas/solid systems with special reference to the determination of surface area and porosity (Recommendations 1984). *Pure Appl. Chem.* **1985,** *57*, 603-619.

TOC GRAPHIC